

Solar volumetric receiver coupled to a parabolic dish: heat transfer and thermal efficiency analysis

**Judit García-Ferrero^a, Rosa P. Merchán^b, María Jesús Santos^c, Alejandro Medina^d,
Antonio Calvo Hernández^e, Paulo Canhoto^f and Andrea Giostri^g**

^a Universidad de Salamanca, Salamanca, Spain, jgferrero@usal.es (CA)

^b rpmerchan@usal.es

^c smjesus@usal.es

^d amd385@usal.es

^e anca@usal.es

^f Universidade de Évora, Évora, Portugal, canhoto@uevora.pt

^g Politecnico di Milano, Milano, Italy, andrea.giostri@polimi.it

Abstract:

Concentrated Solar Power plants are commonly recognized as one of the most attractive options within carbon free power generation technologies because their high efficiency and also because implementation of hybridization and/or storage is feasible. In this work a small-scale system focused on distributed production, in the range of kW_e (5 kW_e to 30 kW_e), is modeled. A parabolic dish collects direct solar power towards a receiver located at its focus. There, the heat transfer fluid increases its temperature for thermal storage or for directly producing electricity at the power block. Thus, this is a crucial component in CSP systems since it greatly influences global efficiency. There is a trade-off in the energy balance within the thermal receiver, since the higher the temperatures it achieves, the higher the radiation losses could be. In this work, a heat transfer analysis for an air volumetric receiver coupled to a parabolic dish is carried out. The solar receiver is modeled under steady-state conditions using a detailed set of equations. The model considers the main losses by convection, conduction and radiation at the glass window and the surrounding insulator. The temperatures and heat transfers along the different receiver zones are computed with a built from scratch in-house code programmed in Mathematica®. The thermal efficiency mainly depends on the incoming solar irradiance at the glass window, the receiver geometry and the type of materials considered, as well as on the ambient temperature. It is expected that this model (precise but not too expensive from the computational viewpoint) could help to identify the main bottlenecks, paving the way for optimization when designing solar volumetric receivers in this kind of systems.

Keywords:

Concentrated Solar Power, Solar receiver, Heat transfer, Parabolic dish, Distributed energy.

1. Introduction

A key element in any concentrated solar power (CSP) system is the solar receiver. It can be considered as a special type of heat exchanger with the aim to convert the input direct solar irradiance into heat for a thermal fluid. Receiver efficiency is essential to obtain a high efficiency in the overall CSP plant and so, commercial interest. Heat transfer processes in the solar receiver are very complicated and during the last years many experimental or simulation studies were conducted in order to propose optimized designs. A recent compilation of those studies is due to Sedighi *et al.* [1].

A particularly interesting application of CSP systems is the possibility of producing distributed electricity at the scale of kW_e, close to the consumption place. Solar dishes, for instance, are capable to perform this task with good efficiencies. A collecting parabolic dish reflects the input solar radiation into a solar receiver located at parabola focus, where it is transferred to a fluid that uses to be a gas running a thermodynamic cycle.

Particularly, Brayton cycles are being investigated due to their promising features as high efficiency, versatility, compactness, and possibility to integrate hybridization or storage schemes. Requirements for solar receivers designed to operate together with Brayton cycles include the necessity to operate at high temperatures (over about 800°C) and relatively high pressures [2].

Pressurized volumetric receivers use closed loops, can be compact and reach large efficiency at large temperatures and pressures adequate for Brayton cycles [3]. Moreover, can operate with gases different from air, as helium, argon, nitrogen or CO₂. Their design continue being a challenge nowadays in order to set the basis for new evolutions of CSP systems, increasingly interesting from an economic perspective. These receivers

are usually closed with a quartz glass window that can reach temperatures about 1200°C and its cooled by the thermal fluid itself or through an extra cooling system [4]. Behind the glass, there is a cavity containing a porous media, the absorber, that is directly impinged by solar radiation. The gas flows through its pores getting a high temperature. Foam can be metallic or ceramic [5]. The first are more economic and can reach temperatures about 1450°C, for instance with Nickel compounds. Other advantages of metal foams include high porosity and specific surface area, as well as, high mechanical strength. Outer walls of the receivers are usually thermally isolated from the ambient to minimize heat losses. Aluminum silicate is a usual material with a low thermal conductivity (around 0.06 W/(m.K) [6]. Bellos *et al.* [7] have reviewed the most recent technologies and advances on cavity receiver designs for solar dish concentrators.

Studies and analysis of solar receivers for solar dish applications include experiments and simulations at different levels. Zhu *et al.* [4, 6] performed both studies for an own design. The experimental study was conducted at Hangzhou, China, and consisted of a compressor, a dish and a receiver with a Ni foam absorber [4]. Variations with time of different parameters as energy and exergy efficiencies, heat losses, temperatures, pressures were performed at real solar conditions in a period with approximately constant direct normal irradiance (DNI). Subsequently, a simplified stationary model for heat transfer in receiver zones was presented [6]. A good agreement between experimental and calculated receiver efficiency (with values about 82%) was obtained.

At a different level of refinement, Wang *et al.* [8] developed a Computational Fluid Dynamics (CFD) model that was validated against experimental measures. A SiC (silicon carbide) absorber was utilized and different porous parameters were analyzed. Maximum temperatures of the outlet air slightly exceeded 1000 K. Solar to thermal efficiencies over 63% were obtained.

The aim of this work is to accurately predict the thermal efficiency of the system made up of a Parabolic Dish Collector (PDC) and a solar volumetric receiver placed at its focus. This system subsequently could be coupled to a thermal cycle, as Stirling or Brayton ones, to produce electric energy for distributed applications. This work is part of a series of studies by our group devoted to a complete modeling of the overall system, including the optics of the parabolic dish, the thermal efficiency of the receiver and the efficiency of the thermodynamic cycle. The methodology intends to be capable of making precise computations for each subsystem at a similar physical level, making clear the bottlenecks of all involved efficiencies with the aim to propose improved designs and operation schemes on the whole system [9]. Special emphasis on subsystems integration is envisaged. For instance, CFD analysis would be an alternative analysis method [10]. However, this would an extensive computational effort and the key physical factors affecting global system efficiency (and the corresponding efficiency bottlenecks) are not always easy to extract. Due to space limitations, in this paper only the model for the efficiency of the solar receiver is exposed.

A detailed set of equations for the heat transfer model in each of the stages during gas heating will be employed. The model includes some features not considered and/or barely touched in previous works, as the volumetric (instead of superficial) heat transfer coefficient for the porous media, different temperatures inside and outside of the glass window, losses across the receiver insulator, more accurate expressions for thermal radiation exchanges and a more complete set of view factors. All these factors are included in appropriate energy balance equations. Most important losses are also incorporated to the model. The models presented in the following paragraphs pursue to be realistic enough to precisely determine the thermal efficiency within a reasonable computational time. They include a comprehensive set of equations with a relatively large number of parameters, but all of them are controllable and with a clear physical origin and meaning.

2. Modelling

The solar receiver model was originally inspired in that from Zhu *et al.* [6], although significant modifications are introduced in order to enlarge its capabilities and to improve model accuracy. The solar receiver model is exposed in the following subsections.

2.1. Energy efficiency equation

The receiver thermal efficiency is the ratio between the heat absorbed by the fluid and the total heat flux impinging at the receiver aperture area, as it is shown in Eq. (1):

$$\eta_{th,rcv} = \frac{\dot{Q}_r}{I_b} = \frac{\dot{m}(\bar{h}_o - \bar{h}_i)}{\eta_d A_d DNI} \quad (1)$$

where \dot{Q}_r stands for the heat flux absorbed by the fluid at the receiver. It can be calculated in terms of the fluid mass flow through the receiver, \dot{m} , and the difference between the outlet and inlet fluid specific enthalpies, \bar{h}_o and \bar{h}_i , respectively. I_b is the solar radiation power impinging at the solar receiver window. This parameter can be expressed as the product of the parabolic dish optical efficiency, η_d , dish aperture area, A_d , and direct solar irradiance (DNI) [6, 11]. Thus, Eq. (1) encompasses solar receiver efficiency associated with heat losses and parabolic dish optical efficiency.

2.2. Solar volumetric modelling: Heat transfer equations

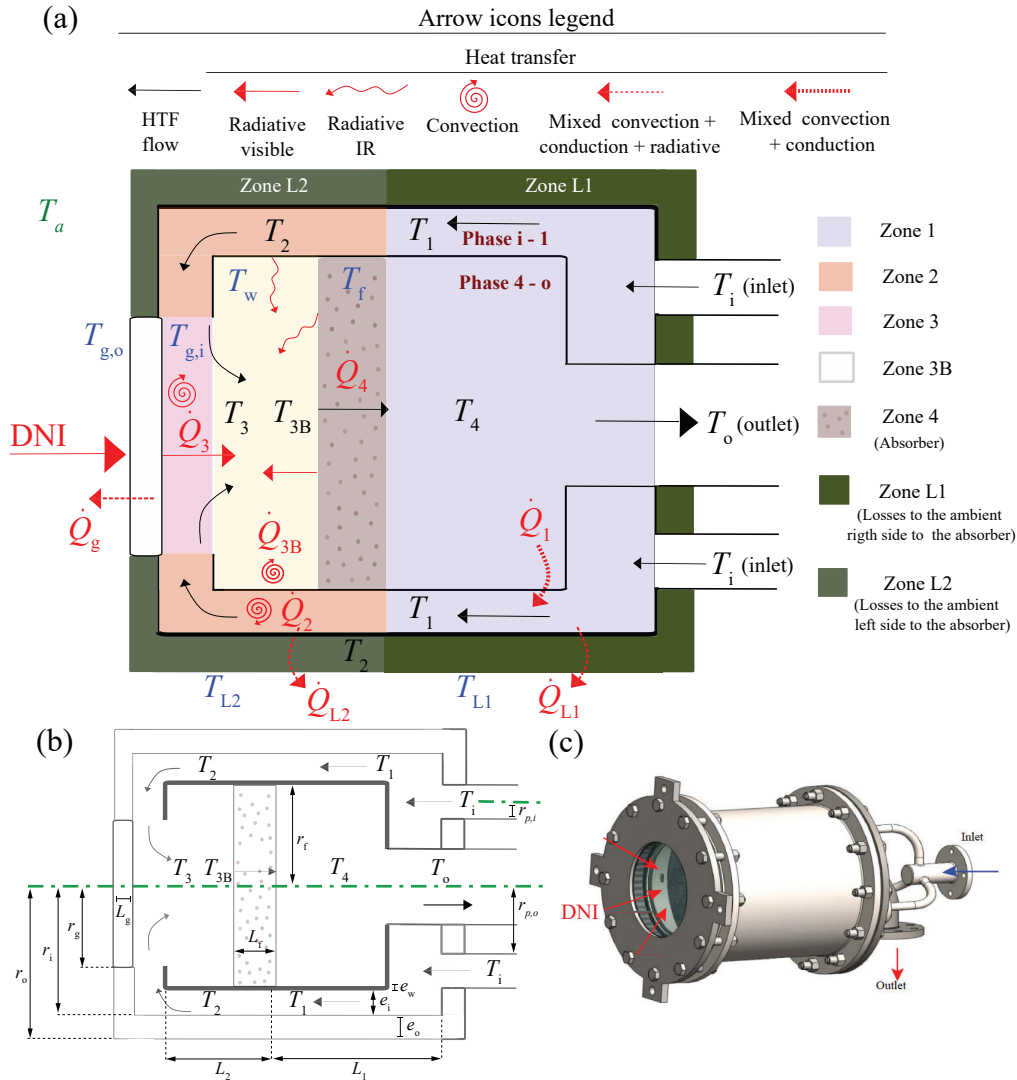


Figure 1: (a) Scheme of the receiver used for this work [6]. Air temperatures ($T_i, T_1, T_2, T_3, T_{3B}, T_4$ and T_o) are depicted in black. Surfaces temperatures related to glass, internal wall, absorber foam, front external insulator, and back external insulator (T_g, T_w, T_f, T_{L1} and T_{L2} , respectively) in blue and ambient temperature (T_a) is depicted in green. (b) Geometrical parameters used in the heat transfer model of the receiver. (c) 3D image of the receiver (taken from Zhu *et al.* [6]).

The solar receiver model presented hereby considers an axially cylindrical pressurized volumetric receiver with a geometrical design as shown in Fig. 1. For validation and numerical applications the design by Zhu *et al.* [6] will be considered, but the models developed in this paper could be applied to other designs and dimensions in a straightforward manner. The symmetry axis goes through the window centre and it is normal to the window surface. As commented in the Introduction, this kind of receivers are especially interesting for high-temperature applications because aperture quartz glasses can reach temperatures quite above 1000°C and receiver thermal efficiency at such conditions can be very high. Usually, the heat transfer fluid (HTF) is pressurized air and the receiver core is a metal or ceramic foam that will be considered as a uniform medium with a given porosity (Zone 4 in Fig. 1).

All the temperatures and heat exchanges involved are included and shown in Fig. 1(a). Figure 1(b) displays the main geometric parameters considered. The HTF (air) enters the receiver at T_i temperature and crosses different zones until it arrives at the outlet, at temperature T_o . Next, a brief description of all zones is given.

- Zone 1: It can be split in two parts: phase $i - 1$ (from the receiver inlet until the end of Zone 1), and phase $4 - o$ (from Zone 1 after the absorbing foam until the receiver outlet). The colder air (at temperature T_i) receives heat (\dot{Q}_1) from the flux of air which is crossing the receiver outlet, since the latter has a higher temperature (T_o). Thus, the air arrives at Zone 2 at temperature T_1 . Due to this heat exchange, the temperature at the receiver exit, T_o , is slightly lower than the air temperature just after crossing the absorber foam (T_4). The heat transfer can be modeled as a mixed convection and conduction process (similar to a heat exchanger).
- Zone 2: There is a heat transfer (\dot{Q}_2) through the inner cylinder wall (at temperature T_w) to the air, which rises its temperature from T_1 to T_2 . \dot{Q}_2 comes from the thermal and visible radiation emitted by the absorber foam and the glass window to the inner cylinder wall.
- Zone 3: The air receives a heat flux \dot{Q}_3 by means of convection with the inner glass surface (at temperature $T_{g,i}$). Thus, the air achieves temperature T_3 . Besides, the heat balance at the glass window has to be considered, and it will be further explained in detail in the following paragraphs.
- Zone 3B: The air exchanges a heat flux, \dot{Q}_{3B} , through convection with the inner wall surface (at temperature T_w). Hence, the air arrives at the absorber foam at temperature T_{3B} . \dot{Q}_{3B} influences the energy balance at Zone 2.
- Zone 4: Here, the fluid crosses the absorber foam (at temperature T_f), receiving thus a heat flux \dot{Q}_4 . In this stage, the air rises its temperature up to T_4 . The heat transfer corresponds to a convection with the pores inside the absorber foam.

The previous brief explanation serves as an introduction to the set of equations employed for simulating the receiver. The equations are exposed in the following paragraphs but first, some considerations should be noticed:

- This work presents a steady-state model. Hence, mass balance equations ($\dot{m}_i = \dots = \dot{m}_o = \dot{m}$) will be indirectly included within heat balance equations.
- Absorber foam (T_f) temperature is considered uniform along the whole material. This assumption means that T_f is the left, right and inside temperature for the absorber foam.
- The wall of the inner cylinder is considered a grey body under thermal-balance conditions. Then, its absorptivity (α_w) and emittance (ϵ_w) are equivalent. This element also possesses a uniform temperature T_w .
- It has been considered negligible the glass thermal radiation transmittance. Thus, there are no radiation losses across the glass (greenhouse effect).

As in any heat transfer process, three equations should be taken into account: heat transfer mechanisms, and mass and energy balances. As previously mentioned, mass balance is included within enthalpy balance. Regarding the pressure, it has been considered a global pressure drop of 0.2 bar [11] across the receiver. However, for each heat transfer, the pressure drop is small enough for considering it constant. Thus, within the equations, the isobaric heat capacity, \bar{c}_p , will be considered instead of enthalpies. The following equations describe the volumetric solar receiver model:

2.2.1. Zone 1

The heat exchange in this zone is modeled as a heat exchanger (Logarithmic Mean Temperature Difference, LMTD, expression will be considered). Then, the energy balance can be written as:

$$\dot{Q}_1 = \dot{m} \bar{c}_p(T)(T_1 - T_i) + \dot{Q}_{L1} = \dot{m} \bar{c}_p(T)(T_4 - T_o) \quad (2)$$

Here, \dot{Q}_{L1} stands for the thermal losses through the insulator (Zone L1, see Fig. 1). Besides, as a heat exchanger, the heat transfer should meet the following relation:

$$\dot{Q}_1 = U_1 A_1 \frac{(T_o - T_i) - (T_4 - T_1)}{\log \frac{(T_o - T_i)}{(T_4 - T_1)}} \quad (3)$$

where $\bar{c}_p(T)$ stands for the average isobaric thermal capacity between temperatures T_i and T_1 , or between T_4 and T_o . $\bar{c}_p(T_m)$ is calculated through REFPROP coupled with Mathematica® [12, 13]. Regarding U_1 , it represents a global conduction and convection heat transfer coefficient, while A_1 stands for the effective Zone 1 area.

2.2.2. Zone 2

The heat transfer in this zone, \dot{Q}_2 , is also modeled as a heat exchanger, where the air and the inner wall cylinder are involved. The energy balance can be written as:

$$\dot{Q}_2 = \dot{m}\bar{c}_p(T)(T_2 - T_1) + \dot{Q}_{L2} = h_{wo}A_w \frac{(T_w - T_1) - (T_w - T_2)}{\log \frac{(T_w - T_1)}{(T_w - T_2)}} \quad (4)$$

where \dot{Q}_{L2} represents the thermal losses through the insulator (Zone L2 in Fig. 1) and T_1 , T_2 are the air temperatures at Zone 1 and Zone 2, respectively. h_{wo} is the convective coefficient at the inner cylinder outer surface wall. A_w stands for the inner cylinder wall area, but it only comprises the wall area in between the absorber foam and the glass window. Temperature T_w is the inner wall temperature.

Finally, heat flux \dot{Q}_2 emitted by the wall comes from the absorber foam and from the glass window. The absorber foam releases thermal and visible radiation due to the reflection of the direct sun beam radiation (I_b) impinging on it. It also receives visible radiation from the glass window. At the same time, the wall losses energy due to the convection with the air crossing Zone 3B, and thermal radiation to the glass window are considered. Then, the following heat balance equation can be written:

$$\dot{Q}_2 = \overbrace{\tau_g I_b F_{gf} \cdot \rho_f F_{fw}}^{\text{Visible radiation from foam}} + \overbrace{\tau_g I_b F_{gw}(1 - \rho_w F_{wf} - \rho_w F_{wg})}^{\text{Visible radiation from glass window}} + \overbrace{\frac{\sigma(T_f^4 - T_w^4)}{\frac{1-\epsilon_f}{A_f \epsilon_f} + \frac{1}{A_f F_{fw}} + \frac{1-\epsilon_w}{A_w \epsilon_w}}}^{\text{Thermal radiation from foam}} - \overbrace{\frac{\sigma(T_w^4 - T_{g,i}^4)}{\frac{1-\epsilon_w}{A_w \epsilon_w} + \frac{1}{A_w F_{wg}} + \frac{1-\epsilon_g}{A_g \epsilon_g}}}^{\text{Thermal radiation to the glass}} - \underbrace{\dot{Q}_{3B}}_{\text{Convection with air}} \quad (5)$$

where ϵ_w , ϵ_f and ϵ_g are the wall, absorber foam and glass window emissivities, respectively. Note that the wall is being considered as a grey body in thermal equilibrium. Thus, the wall absorptivity (*i.e.* the share of energy that the wall will absorb and transfer to the air) is the same as the wall emissivity ($\alpha_w = \epsilon_w$). The share of visible radiation reflected by the foam and by the wall are represented as ρ_f and ρ_w , respectively, while τ_g is the glass window transmissivity. A_f is the cross-sectional foam area, and σ is the Stefan-Boltzmann constant. The term F_{fw} is the 'view factor' between the foam and the wall. It represents the ratio between the amount of thermal radiation leaving the foam that hits the wall [14]. Similarly, F_{wg} is the wall-to-glass view factor, and F_{gf} is the glass-to-foam view factor. Finally, T_f and $T_{g,i}$ are the absorbing foam and the inner glass surface temperatures, respectively. \dot{Q}_{3B} is the convection heat exchange between the inner wall and the fluid, which will be defined later.

2.2.3. Zone 3

Here, the air fluxes over the internal surface of the glass window. This prevents the window breakage, since the air flux lowers its temperature. On one hand, there is a convection heat transfer between the air and the inner window surface, which can also be modeled as a heat exchanger. Thus, the following equations can be used:

$$\dot{Q}_3 = \dot{m}\bar{c}_p(T)(T_3 - T_2) = h_{gi}A_g \frac{(T_{g,i} - T_3) - (T_{g,i} - T_2)}{\log \frac{(T_{g,i} - T_3)}{(T_{g,i} - T_2)}} \quad (6)$$

where h_{gi} is the convective coefficient at the glass inner surface, A_g is the cross sectional glass area, T_g is the glass window temperature and T_3 , T_2 are the Zone 3 and Zone 2 temperatures, respectively.

Besides, some other heat transfers occurs at the glass window. It receives visible radiation directly from the Sun (I_b) as well as from the absorber foam ($\sim F_{fg} \rho_f \tau_g I_b$). The window also receives thermal radiation from the wall and the foam. However, it also suffers convection and radiation losses with the ambient. The convection heat transfer with the air can be also considered a 'loss' at the glass window inner surface. All these phenomena can be summarized in the following expression:

$$\begin{aligned} & \overbrace{\alpha_g \cdot I_b + \tau_g I_b (F_{fg} \rho_f F_{fg} + F_{gw} F_{wg} \rho_w)}^{\text{Visible radiation}} + \overbrace{\frac{\sigma(T_f^4 - T_{g,i}^4)}{\frac{1-\epsilon_f}{A_f \epsilon_f} + \frac{1}{A_f F_{fg}} + \frac{1-\epsilon'_g}{A_g \epsilon'_g}}}^{\text{Thermal radiation from foam}} + \overbrace{\frac{\sigma(T_w^4 - T_{g,i}^4)}{\frac{1-\epsilon_w}{A_w \epsilon_w} + \frac{1}{A_w F_{wg}} + \frac{1-\epsilon'_g}{A_g \epsilon'_g}}}^{\text{Thermal radiation from wall}} = \\ & = \underbrace{\dot{Q}_3}_{\text{Convection with air}} + \underbrace{h_{go} A_g (T_{g,o} - T_a)}_{\text{Convection with ambient}} + \underbrace{\epsilon'_g A_g \sigma (T_{g,o}^4 - T_a^4)}_{\text{Radiation with ambient}} \end{aligned} \quad (7)$$

where α_g is the glass absorptance at visible wavelength. ϵ'_g is the glass emissivity at long wavelength and F_{fg} is the foam-to-glass view factor. Finally, h_{go} stands for the convective coefficient at the outer glass surface.

2.2.4. Zone 3B

Aiming to model the solar receiver as realistic as possible, it has been considered a convection heat exchange between the internal wall, on the inner side, with the fluid. This heat transfer is not considered in [6]. The energy balance equations describing this phenomena will be related to the energy balance at Zone 2 (\dot{Q}_{3B} in Eq. (5)):

$$\dot{Q}_{3B} = \dot{m}c_p(T)(T_{3B} - T_3) = h_{wi}A_w \frac{(T_w - T_3) - (T_w - T_{3B})}{\log \frac{(T_w - T_3)}{(T_w - T_{3B})}} \quad (8)$$

where h_{wi} is the convective coefficient at the wall inner surface, A_w is the internal wall area, T_w is the wall temperature and T_{3B} , T_3 are the Zone 3B and Zone 3 air temperatures, respectively.

2.2.5. Zone 4

At this stage, the absorbing foam exchanges heat with the air crossing through it. This occurs through convection, so the energy balance equations are:

$$\dot{Q}_4 = \dot{m}\tilde{c}_p(T)(T_4 - T_3) = V_f \cdot h_{vf} \frac{(T_f - T_3) - (T_f - T_4)}{\log \frac{(T_f - T_3)}{(T_f - T_4)}} \quad (9)$$

where V_f is the absorber foam vacuum volume $V_f = A_f L_f \phi$. The parameters ϕ and L_f are the foam porosity and foam width, respectively. Zhu *et al.* [4, 6] only provides the pore diameter, d_p , and the Pores Per Inch, (PPI). Thus, Fu *et al.* [15] expression was used for obtaining the absorbing foam porosity: $\phi = (\pi/4)(\text{PPC } d_p)^2$ where PPC refers to 'Pores Per Centimeter'. It can be calculated by means of PPI.

The volumetric convective coefficient, h_{vf} , is obtained by following Barreto *et al.* [10], Wu *et al.* [16] and Fu *et al.* [15] works. Similarly to previous equations, T_4 stands for the air temperature at the foam outlet. Besides, an energy balance for the absorber foam system must be established. The foam absorbs the visible radiation coming from the glass window, but it also suffers some losses: visible radiation reflected, convection heat transfer with the air, and thermal radiation emitted to the wall and glass. So, the following equation can be written:

$$\overbrace{\tau_g I_b F_{gf}(1 - \rho_f)}^{\text{Visible from glass to foam}} + \overbrace{\tau_g I_b F_{gw} \cdot F_{wf} \rho_w}^{\text{Visible from wall to foam}} = \dot{Q}_4 + \overbrace{\frac{\sigma(T_f^4 - T_w^4)}{\frac{1-\epsilon_f}{A_f \epsilon_f} + \frac{1}{A_f F_{fw}} + \frac{1-\epsilon_w}{A_w \epsilon_w}}}^{\text{Thermal radiation to the wall}} + \overbrace{\frac{\sigma(T_f^4 - T_{g,i}^4)}{\frac{1-\epsilon_f}{A_f \epsilon_f} + \frac{1}{A_f F_{fg}} + \frac{1-\epsilon_g}{A_g \epsilon_g}}}^{\text{Thermal radiation to the glass}} \quad (10)$$

The air temperatures at all the stages are perfectly characterized by those previous equations. However, losses through the receiver insulator must be modeled in order to obtain more precision when analyzing the system.

2.2.6. Heat losses at the insulator: Zone L1

This zone refers to the cylindrical insulator from the inlet pipes until the absorber foam plane. It also considers the plane surface surrounding the inlet and outlet pipes, as depicted in Fig. 1. The heat transfer across the insulator surfaces will be modeled as a heat exchanger. So, the heat transferred from the air to the insulator (convection and conduction) must be the same as the heat flux from the outer insulator surface to the surroundings (convection and radiation).

$$\dot{Q}_{L1} = A_{iL1} U_{L1} \frac{(T_1 - T_{L1}) - (T_i - T_{L1})}{\log \frac{(T_1 - T_{L1})}{(T_i - T_{L1})}} \quad (11)$$

where \dot{Q}_{L1} denotes the heat flux that is lost through the Zone L1. A_{iL1} stands for the internal insulator area, including the cylindrical and the circular sectors ones. U_{L1} is an effective heat transfer coefficient, which accounts for the cylindrical and plane zones. Thus, $A_{iL1} U_{L1}$ can be written as:

$$A_{iL1} U_{L1} = A_{iL1.cyl} U_{cyl.L1} + A_{iL1.flat} U_{flat.L1} \quad (12)$$

where:

$$A_{iL1.cyl} = 2 \pi r_i L_1; \quad A_{iL1.flat} = \pi (r_i^2 - r_{p,o}^2 - 3r_{p,i}^2) \quad (13)$$

$$U_{cyl.L1} = \left[\frac{1}{h_{L1,in}} + \frac{r_i \cdot \log(r_o/r_i)}{k_i} \right]^{-1}; \quad U_{flat.L1} = \left[\frac{1}{h_{L1,in}} + \frac{e_o}{k_i} \right]^{-1} \quad (14)$$

$U_{cyl,L1}$ and $U_{flat,L1}$, represent two global conduction and convection heat transfer coefficients for the cylindrical and flat areas, respectively. The insulator thermal conductivity (0.06 W/(m.K) for aluminium silicate) is denoted by k_i , e_o stands for the insulator thickness and $h_{L1,in}$ represents an average convection coefficient for the inner insulator surface. r_i denotes the inner insulator cylinder radius while r_o accounts for the external insulator radius, respectively. $r_{p,i}$ and $r_{p,o}$ are the inlet and outlet pipes radius. The effective flat area, $A_{iL1,flat}$, does not include the three inlet pipes nor the outlet pipe (see Eq. (13)). The last heat exchange occurs at the outer insulator surface, where convection and radiation with the surroundings has been considered. Thus, this phenomenon can be described through the following expression:

$$\dot{Q}_{L1} = A_{o1} (h_{c,L1} + h_{r,L1}) (T_{L1} - T_a) \quad (15)$$

where A_{o1} represents the insulator outer surface area in Zone L1, including cylindrical and flat ones:

$$A_{o1} = A_{o1,cyl} + A_{o1,flat} = 2\pi r_o L_1 + \pi (r_o^2 - r_{p,o}^2 - 3r_{p,i}^2) \quad (16)$$

$h_{c,L1}$ is the convection coefficient between the outer insulator surface temperature (T_{L1}) and ambient temperature (T_a), while $h_{r,L1}$ stands for the radiation coefficient under the same conditions. This radiation coefficient can be written as follows [17]:

$$h_{r,L1} = \epsilon_{L1} \sigma (T_{L1} + T_a)(T_{L1}^2 + T_a^2) \quad (17)$$

where ϵ_{L1} is the outer insulator surface emissivity.

2.2.7. Heat losses at the insulator: Zone L2

This zone refers to the cylindrical insulator from the absorber foam plane until the glass window plane. It also takes into account the plane surface surrounding the glass window, as depicted in Fig.1. Similarly to Zone L1, the heat transfer across the insulator surfaces will be considered as heat exchangers.

$$\dot{Q}_{L2} = A_{iL2} U_{L2} \frac{(T_2 - T_{L2}) - (T_1 - T_{L2})}{\log \frac{(T_2 - T_{L2})}{(T_1 - T_{L2})}} \quad (18)$$

where \dot{Q}_{L2} denotes the heat flux lost through the insulator front side. $A_{iL2} U_{L2}$ is an effective heat transfer coefficient, which accounts for the cylindrical and flat zones.

The coefficients are analogous to those explained for Eqs. (11) and (13). The only difference is that here, the temperatures involved are T_2 , T_1 and T_{L2} (the outer insulator surface temperature in Zone L2) as depicted in Fig. 1. r_g stands for the receiver glass window radius.

Again, the heat released from the outer insulator surface to the surroundings, can be described by:

$$\dot{Q}_{L2} = A_{o2} (h_{c,L2} + h_{r,L2}) (T_{L2} - T_a) \quad (19)$$

where A_{o2} represents the insulator outer surface area within Zone L2, including cylindrical and flat ones.

$h_{c,L2}$ is the convection coefficient between the outer insulator surface temperature (T_{L2}) and ambient temperature (T_a), while $h_{r,L2}$ stands for the radiation coefficient under the same conditions.

2.3. Receiver thermal energy efficiency

All previous equations allow for calculating the receiver efficiency by means of Eq. (1) through the resolution of T_o . However, $\eta_{th,rcv}$ can also be estimated by means of the heat fluxes as follows:

$$\eta_{th,rcv} = \frac{\dot{Q}'_1 + \dot{Q}'_2 + \dot{Q}_3 + \dot{Q}_{3B} + \dot{Q}_4 - \dot{Q}_1}{I_b} \quad (20)$$

where $\dot{Q}'_1 = \dot{Q}_1 - \dot{Q}_{L1}$ and $\dot{Q}'_2 = \dot{Q}_2 - \dot{Q}_{L2}$. Within Zone 1, a wall temperature, T_w , it is not considered, and the inner cylinder wall is assumed to be a heat exchanger. So, note that \dot{Q}_1 is not a net flux since it is gained by the fluid at the inlet (phase $i - 1$) but it is lost at the output (phase $4 - o$). Considering this, Eq. (20) can be rewritten as:

$$\eta_{th,rcv} = \frac{\dot{Q}_2 + \dot{Q}_3 + \dot{Q}_{3B} + \dot{Q}_4 - \dot{Q}_{L1} - \dot{Q}_{L2}}{I_b} \quad (21)$$

Finally, the efficiency can also be expressed as a function of heat losses as follows:

$$\eta_{th,rcv} = 1 - \frac{\dot{Q}_g + \dot{Q}_{L1} + \dot{Q}_{L2} + \rho_g I_b}{I_b} \quad (22)$$

where the term $\rho_g I_b$ accounts for the share of solar energy radiation reflected by the glass window.

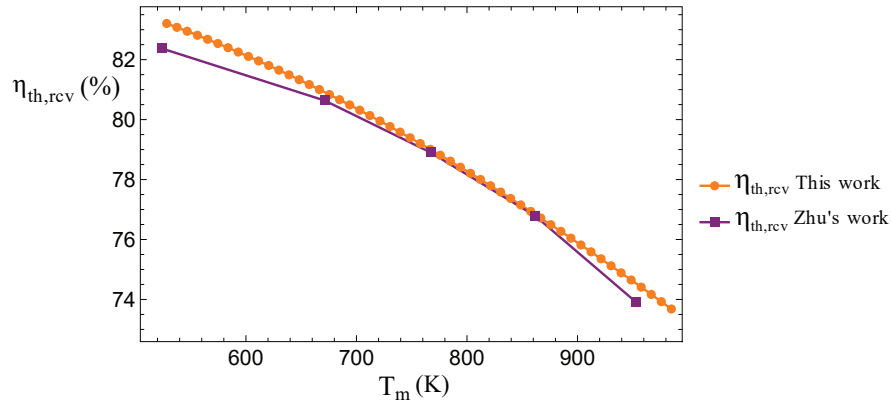


Figure 2: Solar receiver thermal efficiency as a function of mean receiver temperature, T_m : Comparison between Zhu's model (purple) [4] and this work (orange).

3. Validation

In this subsection, the validation of the solar receiver model is presented. As mentioned before, the geometry has been mainly taken from Zhu's work [4]. The optical efficiency will be taken as the same that Zhu *et al.* provide ($\eta_d = 0.8645$). In Table 1, the value of the parameters employed for the validation process are exposed. In Fig. 2, a comparison between the values obtained in this work and Zhu *et al.* [6] results is depicted. It shows a good agreement, especially in the medium zone of the temperature interval. The smallest relative difference (0.05%) is found at 861.8 K. The greater relative differences are found at the lowest temperature (1.06% at 523.9 K) and at the highest temperature (0.83% at 953.3 K). The relative difference is below 1.5% for all the cases. Thus, it can be considered that the model presented here has been validated.

4. Application

The model presented here can be used to predict the thermal receiver efficiency at specific locations with different meteorological conditions. In Fig. 3, the receiver thermal efficiency for two days is presented. The mass flow rate remains constant in these simulations. The location selected is Ouarzazate (Morocco) and the days are one day in summer (June 24th, 2021) and one day in winter (December 22th, 2021). The variation of DNI and ambient temperature (T_a) are also attached.

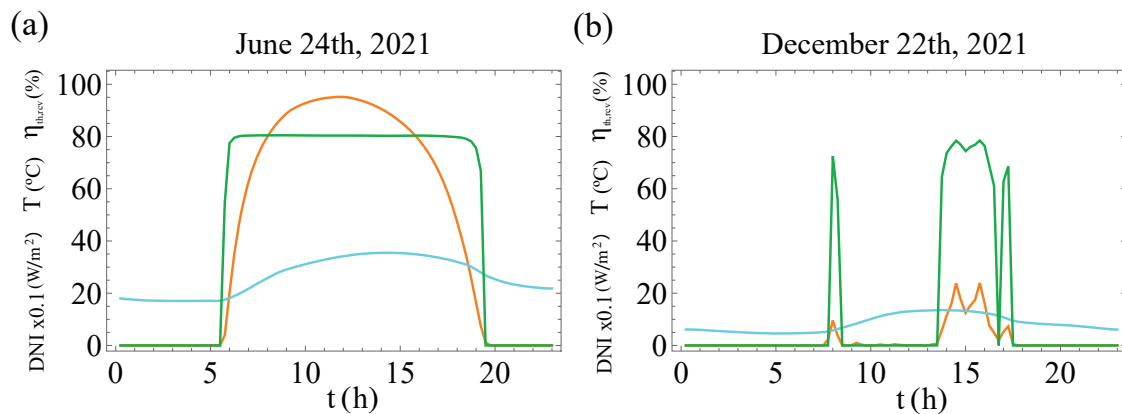


Figure 3: Solar receiver thermal efficiency along one day at Ouarzazate (Morocco). The thermal receiver efficiency, ($\eta_{th,rev}$, (%), green), DNI (W/m^2) multiplied by 0.1 (orange) and ambient temperature ($^{\circ}C$, cyan) are depicted together. (a) June 24th, 2021. (b) December 22th, 2021. December month is exposed for proving that, if DNI overcome a minimum value, receiver's thermal efficiency could achieve values close to the ones obtained in summer.

Table 1: Solar receiver parameters for the validation with Zhu's [6] work.* These parameters are not made explicit within Zhu's work.

Nomenclature	Value (unit)	
DNI	600 W/m ²	Solar heat flux impinging at the glass window
σ	5.67 · 10 ⁻⁸ W/(m ² K ⁴)	Stefan Boltzmann constant
\dot{m}	0.04 kg/s	Mass flow rate
η_d	0.8645	Dish optical efficiency
A_d	44 m ²	Dish aperture area
Glass window		
ρ_g	0.136	Reflectivity at visible wave
τ_g	0.851	Transmissivity at visible wave
α_g	0.013	Absorptivity at visible wave
* α'_g	1	Absorptivity at long wave (perfect)
r_g	0.125 m	Radius
* L_g	0.015 m	Glass thickness
Inner cylinder wall		
ρ_w	0.2	Reflectivity at visible wave
ϵ_w	0.8	Emissivity (grey body at thermal equilibrium)
A_w	0.1788 m ²	Total wall area (only the share of wall placed in between porous matrix and glass window)
* e_w	0.001 m	Wall thickness
Foam porous matrix		
ρ_f	0.05	Reflectivity at visible wave
ϵ_f	0.95	Emissivity (grey body at thermal equilibrium)
r_f	0.182 m	Radius
L_f	0.065 m	Foam width
ϕ	0.792 (-)	Porosity
PPI / PPC	75 / 29.53	Pores Per Inch / Pores Per Centimeter
d_p	3.40 · 10 ⁻⁴ m	Pore diameter
d_c	1.86 · 10 ⁻³ m	Average pore cell diameter
l_s	6.58 · 10 ⁻⁴ m	Strut length
Geometrical parameters*		
L_1	0.195 m	Receiver length for the phase i – 1 (to the right of the foam)
L_2	0.1079 m	Receiver length for the phase 1 – 2 (to the left to the foam)
e_i	0.014 m	Radius difference between inner wall and insulator cylinders
r_i	0.136 m	Internal insulator radius
e_o	0.003 m	Insulator thickness
r_o	0.2 m	External insulator radius
Inlet and outlet pipes		
$r_{p,i}$	0.01 m	Inlet pipe radius
* $r_{p,o}$	0.042 m	Outlet pipe radius
View factors		
F_{fg}	0.4193	Foam porous matrix to glass window
F_{fw}	0.5807	Foam porous matrix to inner wall
F_{gf}	0.8891	Glass window to foam porous matrix
F_{gw}	0.1109	Glass window to inner wall
F_{wf}	0.6069	Inner wall to foam porous matrix

Meteorological data were taken from MERRA (Modern-Era Retrospective Analysis) for the ambient temperature and from Copernicus Europe's eye on earth for the DNI data. Both of them were provided by Solar Radiation Data (SoDa) Service [18, 19]. If the DNI overcomes the minimum value of 30 W/m^2 (necessary for the set of equations to converge), the receiver thermal efficiency ranges between 80.47 % and 54.57 % in June, and between 78.45 % and 56.01 % in December.

The results in Fig. 3(a) shows an almost constant value for $\eta_{th,rcv}$ during the central hours of the day (a sunny day without DNI oscillations), reaching values above 82%. The day selected in December is a cloudy day with strong oscillations of DNI. Mean temperature is quite lower than in June. In spite of this, maximum thermal efficiency value is 78.45 % (only 2.42% below the maximum for June, achieved at a DNI value of 768 W/m^2).

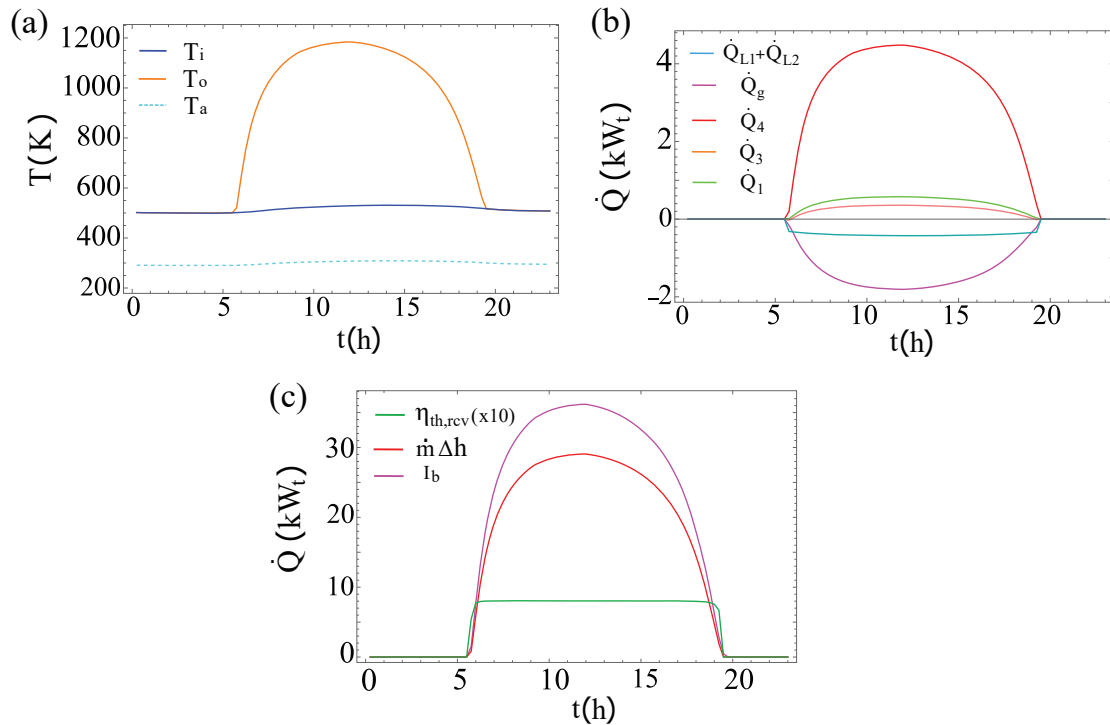


Figure 4: Solar receiver outputs throughout the day June 24th, 2021, at Ouarzazate (Morocco). (a) Inlet (orange), outlet (blue) and ambient temperatures (cyan) in K (T_i , T_o and T_a , respectively). (b) Fluid Heat fluxes (\dot{Q}_1 (green), \dot{Q}_3 (orange), \dot{Q}_4 (red) and losses through the glass window (\dot{Q}_g (magenta) and through the insulator $\dot{Q}_{L1} + \dot{Q}_{L2}$ (dark cyan)). \dot{Q}_4 is multiplied by $0.2 \cdot 10^{-3}$ and \dot{Q}_g is multiplied by 10^{-3} . (c) Thermal receiver efficiency, ($\eta_{th,rcv}$ in green), is multiplied by 10. The product of mass flow and enthalpy increase ($\dot{m} \cdot \Delta h$) (red) and the solar power at the receiver window, I_b (magenta) are depicted together.

In Fig. 4, some of the output indicators of the receiver model throughout June 24th, 2021 are presented. It has been considered that during night hours, and also for DNI values below 30 W/m^2 , the system is turned off. Fig. 4(a) depicts the inlet and outlet temperature (T_i (blue) and T_o (orange), respectively). While T_i seems to follow ambient temperature (T_a) shape (plotted in cyan), the outlet temperature resembles the shape of DNI during the sunlight hours. In Fig. 4(b) it is clear that the heat absorbed inside the porous foam, \dot{Q}_4 (red), is the highest heat flux contribution to the fluid for raising its temperature. At the same time, the heat losses through the glass window, \dot{Q}_g (magenta), account for the main losses within the receiver. In Fig. 4(c), aiming to explain the receiver efficiency plateau during the day, the numerator of the Eq. 1, $\dot{m}(\bar{h}_o - \bar{h}_i)$ was depicted in red, along with the denominator, I_b (magenta). Since the ratio between the numerator and the denominator is almost the same throughout the sunlight hours, the receiver efficiency, $\eta_{th,rcv}$, is also approximately constant during the same hours as it is seen in Fig.4(c) and Fig. 3(a).

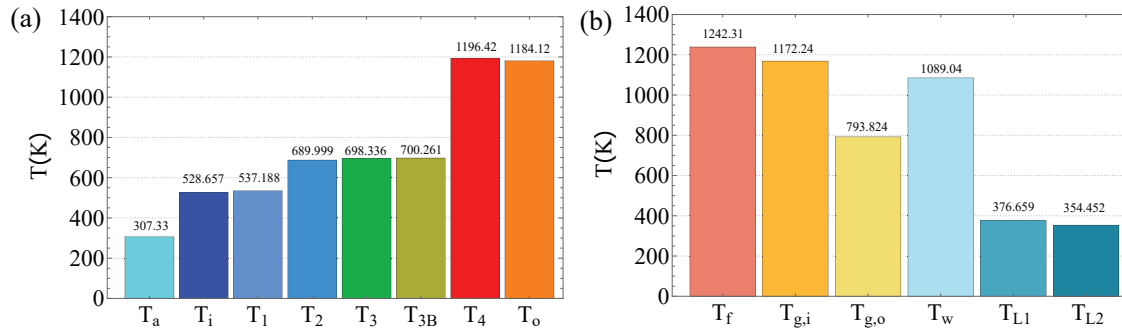


Figure 5: (a) Fluid temperatures during its flow through the receiver (see Fig. 1(a)) for notation. (b) Temperatures on receiver surfaces at the same conditions: June 24th, 2021 at noon.

Finally, in Fig. 5, the profile of the fluid (Fig. 5(a)) and receiver surfaces temperatures (Fig. 5(b)) are shown. These temperature values correspond to June 24th, 2021 at noon (12 h). In Fig. 5(a), it is depicted how the air rises its temperature from 528.7 K (T_i , temperature at the outlet of the initial compressor) until 1196.42 K (T_4 , the temperature after crossing the porous foam). The outlet temperature (T_o) is approximately 12.3 K below T_4 , due to the heat exchange between the receiver outlet and inlet (Zone 1). As depicted in Fig. 5(b), the highest temperature among the surfaces is achieved at the porous foam, T_f , (1242.31 K). There is a difference of 378 K between the inner and outer glass surfaces ($T_{g,i}$ and $T_{g,o}$, respectively). This temperature difference is proportional to the heat losses across the glass window (\dot{Q}_g). The insulator surface temperatures for Zone L1 (376.66 K) and Zone L2 (354.45 K), are about 70 K above ambient temperature. The wall surface temperature (1089.04 K) is close to the inner glass window surface temperature, but it never overcomes it.

5. Conclusions

A physical model for heat transfers and losses in a closed pressurized solar receiver associated to a parabolic dish, small-scale, CSP system was presented. It can be applied to different receiver geometries and materials at stationary conditions. Particularly, a quartz glass on the window and a metallic foam in the absorber were considered. All the main heat transfer efficiencies are modeled and computed, allowing for a precise estimation of receiver thermal efficiency without paying an excessive computational effort. The physical mechanisms influencing receiver efficiency are identified and modeled within realistic hypotheses. This permits to calculate, for any value of DNI and ambient temperature, the temperatures of the heat transfer fluid and receiver surfaces at any stage, and also, to quantify heat transfer flows and losses to the ambient.

The ultimate goal of this kind of models is to couple it with submodels for the optical efficiency of the dish, for instance by means of a ray tracing software like Tonatiuh [20] and also with thermodynamic models for the power unit associated, as Brayton or Stirling cycles. Thus, it would be possible to analyze the behaviour of the whole system and to propose improvements for design or operation with enough precision and without applying to techniques requiring a huge computational effort.

Acknowledgments

Financial support from the Institute of Fundamental Physics and Mathematics (IUFFYM) and Escuela de Doctorado “Studii Salamantini” from University of Salamanca is acknowledged. “European Union, *Next Generation EU*” financial support, within ‘Programa Investigaci3n, Plan de Recuperaci3n, Transformaci3n y Resiliencia’, Junta de Castilla y Le3n and Universidad de Salamanca is also acknowledged. SoDa Transvalor/MINES ParisTech is acknowledged for the meteorological and solar radiation data provided.

References

- [1] M. Sedighi, R. Vasquez Padilla, R.A. Taylor, M. Lake, I. Izadgoshasb, and A. Rose. High-temperature, point-focus, pressurised gas-phase solar receivers: A comprehensive review. *Ener. Conv. Manage.*, 185:678–717, 2019.
- [2] R. P. Merch3n, M. J. Santos, A. Medina, and A. Calvo Hern3ndez. High temperature central tower plants for concentrated solar power: 2021 overview. *Renew. Sust. Ener. Rev.*, 155:111828, 2022.
- [3] M. Lubkoll, T.W. von Backstr3m, and D.G. Kr3ger. Survey on pressurized air receiver development. In *Sol. Ener. Conference*. Sol. Ener. Conference, 2014.

- [4] J. Zhu, K. Wang, G. Li, H. Wu, Z. Jiang, F. Lin, and Y. Li. Experimental study of the energy and exergy performance for a pressurized volumetric solar receiver. *Applied Thermal Engineering*, 104:212–221, 2016.
- [5] V. R. Patil, F. Kiener, A. Grylka, and A. Steinfeld. Experimental testing of a solar air cavity-receiver with reticulated porous ceramic absorbers for thermal processing at above 1000°C. *Sol. Ener.*, 214:72–85, 2021.
- [6] J. Zhu, K. Wang, Z. Jiang, B. Zhua, and H. Wu. Modeling of heat transfer for energy efficiency prediction of solar receivers. *Energy*, 190:116372, 2020.
- [7] E. Bellos, E. Bousi, C. Tzivanidis, and S. Pavlovic. Optical and thermal analysis of different cavity receiver designs for solar dish concentrators. *Ener. Conv. Manage. X*, 2:100013, 2019.
- [8] P. Wang, J. B. Li, F. W. Bai, D. Y. Liu, C. Xu, L. Zhao, and Z. F. Wang. Experimental and theoretical evaluation on the thermal performance of a windowed volumetric solar receiver. *Energy*, 119:652 – 661, 2017.
- [9] R. P. Merchán, M. J. Santos, I. Heras, J. Gonzalez-Ayala, A. Medina, and A. Calvo Hernández. On-design pre-optimization and off-design analysis of hybrid Brayton thermosolar tower power plants for different fluids and plant configurations. *Renew. Sust. Energy Rev.*, 119:109590, 2020.
- [10] Germilly Barreto, Paulo Canhoto, and Manuel Collares-Pereira. Three-dimensional CFD modelling and thermal performance analysis of porous volumetric receivers coupled to solar concentration systems. *Applied Energy*, 252:113433, 2019.
- [11] A. Giotri and E. Macchi. An advanced solution to boost sun-to-electricity efficiency of parabolic dish. *Solar Energy*, 139:337–354, 2016.
- [12] E. W. Lemmon, M. L. Huber, and M. O. McLinden. NIST Standard Reference Database 23: Reference fluid thermodynamic and transport properties-REFPROP, version 9.1. National Institute of Standards and Technology, Standard Reference Data Program, Gaithersburg, 2013.
- [13] Wolfram Research, Inc. Mathematica, Version 13.2. Champaign, IL, 2022.
- [14] Michael F. Modest. *Radiative Heat Transfer*. Academic Press, Elsevier Science, second edition, 2003.
- [15] X. Fu, R. Viskanta, and J.P. Gore. Measurement and correlation of volumetric heat transfer coefficients of cellular ceramics. *Experimental Thermal and Fluid Science*, 17:285–293, 1998.
- [16] Z. Wu, C. Caliot, G. Flamant, and Z. Wang. Numerical simulation of convective heat transfer between air flow and ceramic foams to optimise volumetric solar air receiver performances. *International Journal of Heat and Mass Transfer*, 54:1527–1537, 2011. Issues 7–8.
- [17] Soteris A. Kalogirou. *Solar energy engineering: processes and systems*. Second edition, 2014.
- [18] Global Modeling and Assimilation Office (GMAO) (2015), MERRA-2 tavg1_2d_slv_Nx: 2d,1-Hourly,Time-Averaged,Single-Level,Assimilation,Single-Level Diagnostics V5.12.4, Greenbelt, MD, USA, Goddard Earth Sciences Data and Information Services Center (GES DISC), Accessed 23/02/2023 <https://www.soda-pro.com/web-services/meteo-data/merra>.
- [19] Copernicus atmosphere monitoring service (ECMWF), 2023. Accessed 23/02/2023. <https://www.soda-pro.com/web-services/radiation/cams-radiation-service>.
- [20] M. J. Blanco, J. M. Amieva, and A. Mancillas. The Tonatiuh software development project: An open source approach to the simulation of solar concentrating systems. In *ASME 2005 International Mechanical Engineering Congress and Exposition*, pages 157–164. American Society of Mechanical Engineers., 2005.